Acta Materialia 106 (2016) 59–65

Contents lists available at ScienceDirect

Acta Materialia

journal homepage: www.elsevier.com/locate/actamat

Full length article

Phase-field study of zener drag and pinning of cylindrical particles in polycrystalline materials

Christian Schwarze, Reza Darvishi Kamachali*, Ingo Steinbach

Interdisciplinary Centre for Advanced Materials Simulation (ICAMS), Ruhr-University Bochum, 44801 Bochum, Germany

ARTICLE INFO

Article history:
Received 28 August 2015
Received in revised form
28 October 2015
Accepted 30 October 2015
Available online xxx

Keywords:
Phase-field model
Grain growth
Zener drag and pinning
Young's law

ABSTRACT

Zener drag and pinning in composites reinforced with cylindrical particles is investigated using three-dimensional phase-field simulations. Detailed systematic studies clarify the effect of relative orientation of the particle and length/diameter ratio on the kinetics of drag. It is shown that a combination of local equilibrium at junctions in contact with the particles, initial driving force of the migrating grain boundaries, and configuration of the particles within the polycrystalline matrix determine the intensity and persistence of drag and pinning effects.

1. Introduction

Today industrial materials are in need of excellent physical, chemical and processing properties that are obtained by combining prominent properties of two or more pure substances to fulfill requirements in endless applications [1,2]. The excellent mechanical, electrical and thermal properties of added materials, such as carbon nanotubes [3–5], promise stronger reinforced composites with better functional properties. The microstructure evolution of such composites is of fundamental and technological interest [6–8]. The grain growth resistance in metal matrix composites is well-investigated for secondary particles of spherical and ellipsoidal shapes [9–12], while the behaviour of deviating shapes is still poorly understood. Here, we focus on the effect of particles with large length/diameter ratio, resembling cylinders which are less investigated in the literature but largely used in composite materials.

Previous investigations of particle drag and pinning are mostly concerned with randomly distributed particles with spherical [9,10,13], ellipsoidal [11,12], and cubic shapes [14]. Cylindrical particles have some properties of both spherical and cubic particles with a much larger length/diameter ratio. It is, for instance, application-relevant to know whether longer cylinders have an advantage over shorter ones and if orientation plays a role in the pinning of grain boundaries. Furthermore, in composite materials the strengthening particles are usually distributed non-randomly due to the production process.

Theoretical studies on the shape of particles suggest an increase of maximum pinning force F with deviation from spherical shape, depending on the orientation [15]. Rym and coworkers [12] studied an ellipsoidal particle with a–a–b axes and the shape factor $\varepsilon = b/a$. The moving interface is assumed to be aligned parallel to the a–a plane of the ellipsoid (case 1) or parallel to the a–b plane (case 2):

$$F_{Sphere} = \pi\sigma R, \tag{1}$$

$$\text{Case 1: } F_{Ellipsoid} = F_{Sphere}\,\frac{2\varepsilon^{-1/3}}{(1+\varepsilon)}, \tag{2}$$

$$\text{Case 2: } F_{Ellipsoid} = F_{Sphere}\,\varepsilon^{0.47}, \tag{3}$$

$$F_{Cube} \approx 1.45\,F_{Sphere} \tag{4}$$

with R the radius of the sphere and σ the grain boundary energy. The force of an ellipsoidal particle at constant volume depends on its orientation with respect to the grain boundary. Cuboidal particles have a higher pinning force as long as $\varepsilon < 0.619$ for case 1 and $\varepsilon < 2.204$ for case 2. The overall drag effect, however, depends not

* Corresponding author.
E-mail address: reza.darvishi@rub.de (R. Darvishi Kamachali).

http://dx.doi.org/10.1016/j.actamat.2015.10.045
1359-6454/

only on the pinning force, which is a static measurement of maximum area reduction, but also on the kinetics of the migrating grain boundary and the dynamics of interaction. Moreover, within a polycrystalline body, particles can sit in various locations and also have a cooperative impact on the network of grain boundaries. These aspects can be studied using simulation methods which can consider any geometry of particles and resemble the dynamics of moving boundaries as well as equilibria at the junctions in a physically sound picture.

The aim of the current work is to study Zener drag and pinning of cylindrical particles embedded in polycrystalline materials using the multi-phase-field method [16], which allows studying simultaneous evolution of grain boundaries and junctions next to the particles. We first investigate interaction with a single grain boundary and the effect of orientation, driving force, and formation of triple junctions. Later we study drag and pinning for particles sitting in different positions in the grain boundary network, and the cooperative drag effects in a polycrystalline body. Finally, we discuss pinning of cylinders of different length in polycrystalline bodies.

2. Multi-phase field model and simulation details

The multi-phase-field approach [16–18] applies to studying two or more phases (or grains) in contact where the phase-field variables are constrained to

$$\sum_{\alpha=1}^{N}\phi_\alpha = 1, \tag{5}$$

where $\phi_\alpha \in [0,1]$ and N is the number of existing domains. Previous studies have shown the ability of this method to reconstruct junctions at the equilibrium [19,20] and to study grain growth in polycrystalline materials [21,22]. The multi-phase field model starts with the total free energy functional F_{total} over a given domain Ω:

$$F_{total} = \int_\Omega \left(f^{GB} + f^{CH} + f^{EL} + \ldots\right) \mathrm{d}V, \tag{6}$$

where f^{GB} is the interfacial free energy density, f^{CH} the chemical free energy density and f^{EL} the elastic free energy density. In the present work, the interfacial free energy density is the only contribution of interest expressed in pairs

$$f^{GB} = \sum_{\alpha=1}^{N}\sum_{\beta\neq\alpha}^{N}\frac{4\sigma_{\alpha\beta}}{\eta}\left\{-\frac{\eta^2}{\pi^2}\nabla\varphi_\alpha\cdot\nabla\varphi_\beta + \varphi_\alpha\varphi_\beta\right\}, \tag{7}$$

where η is the interface width and $\sigma_{\alpha\beta}$ is the interfacial energy between domains α and β. The temporal evolution of the phase-field variables follows [23].

$$\dot{\varphi}_\alpha = -\sum_{\beta=1}^{N}\frac{\mu_{\alpha\beta}}{N}\left(\frac{\delta}{\delta\varphi_\alpha} - \frac{\delta}{\delta\varphi_\beta}\right)F_{total}, \tag{8}$$

where $\mu_{\alpha\beta}$ is the interfacial mobility. Using Equations (6)–(8) we obtain

$$\dot{\varphi}_\alpha = \sum_{\beta\neq\alpha}^{N}\frac{\mu_{\alpha\beta}}{N}\left\{\sigma_{\alpha\beta}(I_\alpha - I_\beta) + \sum_{\gamma\neq\alpha,\beta}^{N}(\sigma_{\beta\gamma} - \sigma_{\alpha\gamma})I_\gamma\right\}, \tag{9}$$

in which the generalized curvature term is given by $I_\alpha = \nabla^2\phi_\alpha + \frac{\pi^2}{\eta^2}\phi_\alpha$.

2.1. Simulation procedure

For all simulations the same physical dimensions are chosen. Common light-metal interfacial energy $\sigma_{\alpha\beta}$ and mobility $\mu_{\alpha\beta}$ are taken as 0.32 $\mathrm{Jm^{-2}}$ and 3×10^{-16} $\mathrm{m^4J^{-1}s^{-1}}$ [24], respectively. The interfacial energies between all phases and grains are the same. Time step dt and grid spacing Δx are 1 s and 10^{-9} m, respectively. The width of the interface is benchmarked and selected as $\eta = 7\Delta x$ to guarantee high accuracy and reasonable computation time. The size of the simulation box depends on the type of investigation: for studying drag of a single cylinder we use a box size of 180^3 and $150^2\times250$ grid cells, and for studying polycrystalline composites we use a box size of 512^3 grid cells. The cylinder radius is 7.5 nm and the maximum cylinder length is 100 nm. It is well-known that particles can break during manufacturing processes, e.g., ball-milling before sintering, which results in shorter particles which are investigated here. Particles are arranged both randomly and ordered in direction and position, and the contact between them is prohibited.

For a systematic investigation of anisotropic interaction, we performed simulations with different orientations between the particle and a flat grain boundary driven by an artificial driving force $\Delta G_{\alpha\beta}$. This driving force adds to the kinetic Equation (9) for $\dot{\phi}_\alpha$ as $\mu_{\alpha\beta}h(\phi_\alpha)\Delta G_{\alpha\beta}$. Thus, the velocity of the flat interface between grain α and β is given as

$$v = \frac{\mathrm{d}x}{\mathrm{d}t} = \frac{\partial\phi_\alpha}{\partial t}\frac{\partial x}{\partial\phi_\alpha} = \mu_{\alpha\beta}\frac{\partial x}{\partial\phi_\alpha}h(\phi_\alpha)\Delta G_{\alpha\beta}. \tag{10}$$

In order to have a simple linear relationship between v and $\Delta G_{\alpha\beta}$, we have chosen $h(\phi_\alpha) = \partial\phi_\alpha/\partial x$. For the double obstacle potential used in our model

$$h(\phi_\alpha) = \frac{\partial\phi_\alpha}{\partial x} = \frac{\pi}{\eta}\sqrt{\phi_\alpha\phi_\beta} \tag{11}$$

and thus $v = \mu_{\alpha\beta}\Delta G_{\alpha\beta}$.

For numerical stability, the driving force should be restricted to $\Delta G_{\alpha\beta} < 2\pi\sigma/\eta$ [25]. Note that if, for example, the interface is moving towards grain β (α is growing), $\frac{1}{2}\mu_{\alpha\beta}h(\phi_\alpha)\Delta G_{\alpha\beta}$ is added to $\dot{\phi}_\alpha$ and $-\frac{1}{2}\mu_{\alpha\beta}h(\phi_\alpha)\Delta G_{\alpha\beta}$ to $\dot{\phi}_\beta$. To ensure the stability of the cylinder particles as an inert phase, related interfacial mobility is reduced by a factor of 10^{-25} compared to boundaries between grains.

3. Results and discussion

3.1. Effect of orientation and grain boundary kinetics on the drag

Cylindrical particles are expected to have an orientation-dependent Zener effect, similar to that of ellipsoidal [15] and cubic particles [14]. Here, we analyse the interaction between a moving boundary and a cylindrical particle with different orientation angles. We measure the in-contact boundary velocity, which is the distance travelled by the grain boundary while being in contact with the cylinder divided by the time of interaction between boundary and cylinder. Thus, we are able to discuss not only the drag effect but also the dynamics of the grain boundary depending on its driving force during the interaction. For a cylindrical particle, there is one degree of freedom for the contact angle with respect to a flat grain boundary, as shown in Fig. 1a.

The results show that the drag effect depends on the particle orientation mainly when $\theta < 45°$ (Fig. 1b and c). At low driving forces (Fig. 1b) for $\theta < 20°$ and at high driving forces (Fig. 1c) for $\theta < 8°$, the in-contact velocity significantly drops and particle drag becomes more efficient than a spherical particle of the same

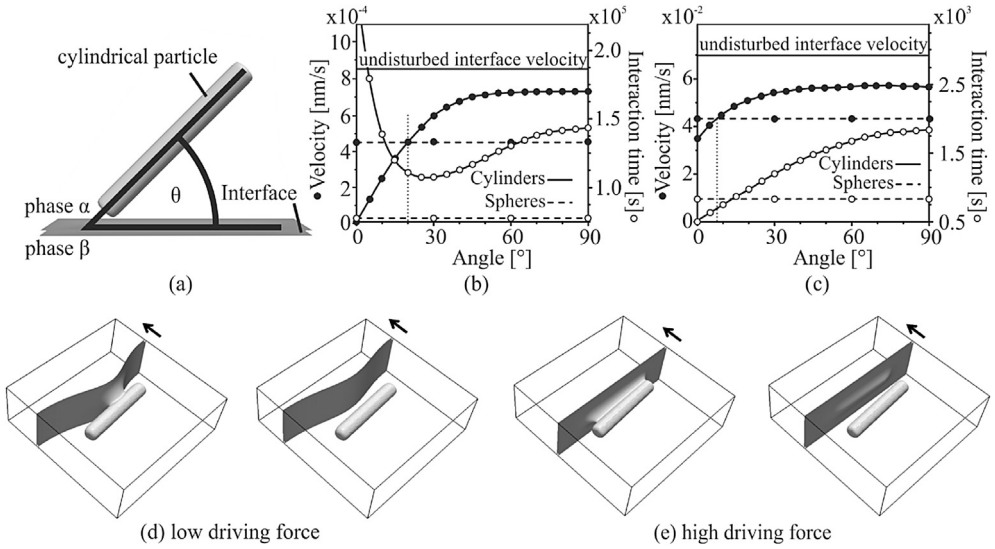

Fig. 1. (a) Schematic of interaction between a grain boundary and a cylindrical inclusion. Grain boundary velocity (filled circles) and contact time (unfilled circles) as a function of orientation for (b) low ($\Delta G = 0.02\pi\sigma/\eta$) and (c) high ($\Delta G = 1.56\pi\sigma/\eta$) driving force compared with a spherical particle. Cylinder length: 100 nm, cylinder radius: 7.5 nm, sphere has the equivalent volume. Detaching of the grain boundary from the particle at $\theta = 10°$ with low (d) and high (e) driving force. Black arrows show moving direction.

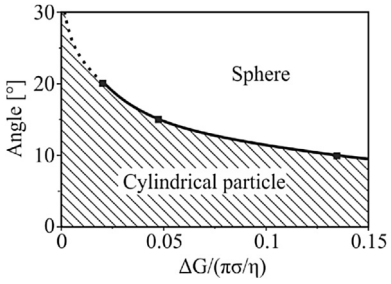

Fig. 2. Mapping effective pinning shape as a function of orientation and driving force. Cylindrical and spherical particles have the same volume.

volume. In fact, if the θ angle is decreased, both the effective in-contact area and the drag effect increase (Fig. 1b and c). Upon interaction, a triple junction forms in the contact plane. Hence, a natural drag is introduced by the junction, similar to that in grain growth predicted by Mullins [26] (see also [25]). The triple junction drag adds to the particle drag and therefore an offset in the velocity, even for $\theta = 90°$ (Fig. 1b and c), is observed. The junction drag is generic and exists all along interaction. This has been, indeed, disregarded in the previous pinning studies until recently, when analytically considered by Zhao and coworkers [27].

Interestingly, it is observed that the driving force of the grain boundary significantly affects drag behaviour. The grain boundary sticks to the particle when the driving force is small. In this case it

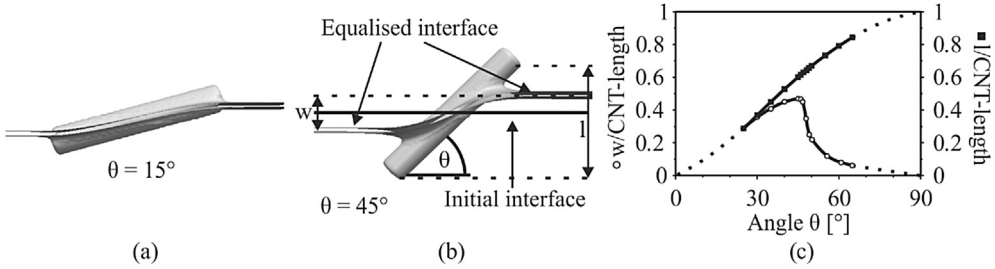

Fig. 3. Equilibrium contact (no driving force) between the grain boundary and the particle (3D) at (a) θ=15° and (b) θ=45°. Dilatation (w) of the grain boundary, and normal length of the cylinder (l) measured as a function of θ (c).

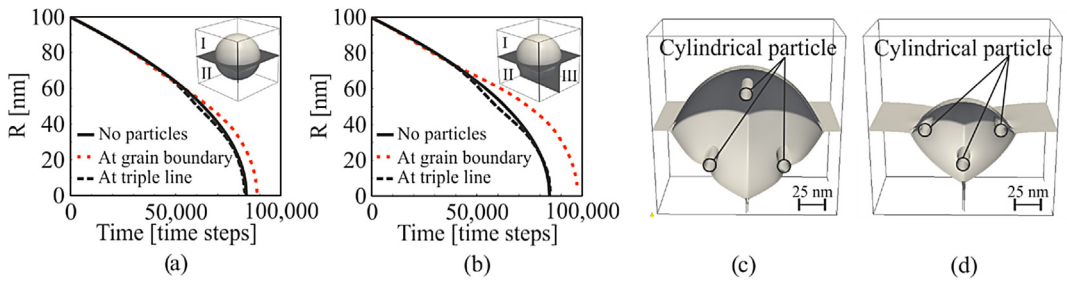

Fig. 4. Kinetics of shrinkage for different inclusion positions for the central, initially spherical grain having (a) two and (b) three neighbouring grains. The simulation box is shown for particles (c) on grain boundaries and (d) on triple junctions. R is the radius of a sphere of equal volume to the central grain.

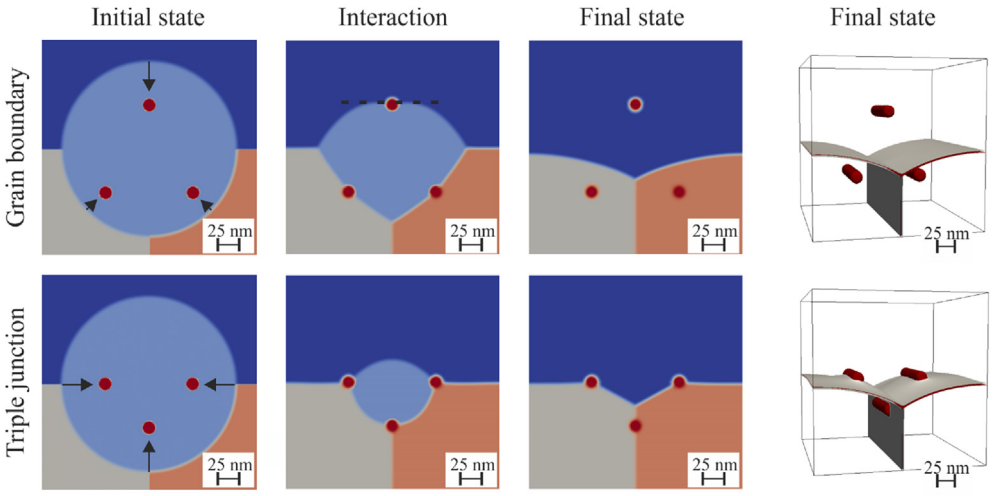

Fig. 5. Slice of 3D shrinking at different time steps and 3D microstructure at final state. Top: Grain boundaries touch the particle and locally straighten around it. Bottom: Cylindrical particles meet triple lines and form three new junctions.

can leave the particle only by severe deformation which happens over a relatively long period of time (Fig. 1b and d). Fig. 1d and e compare detachment of the grain boundary at low and high driving forces. Although the grain boundary faces difficulties at lower driving forces, its migration accelerates due to the deformation once it is detached from the particle. Fig. 2 maps the efficiency of interaction as a function of orientation and driving force. For certain combinations of orientation and driving force values, it is found that a cylindrical particle drags better than a sphere of the same volume.

One feature of cylindrical particles is their orientation-dependent contact with the grain boundary. Fig. 3a and b shows static equilibrium that is governed only by local minimization of the energy, in the absence of a driving force. On the one hand, the

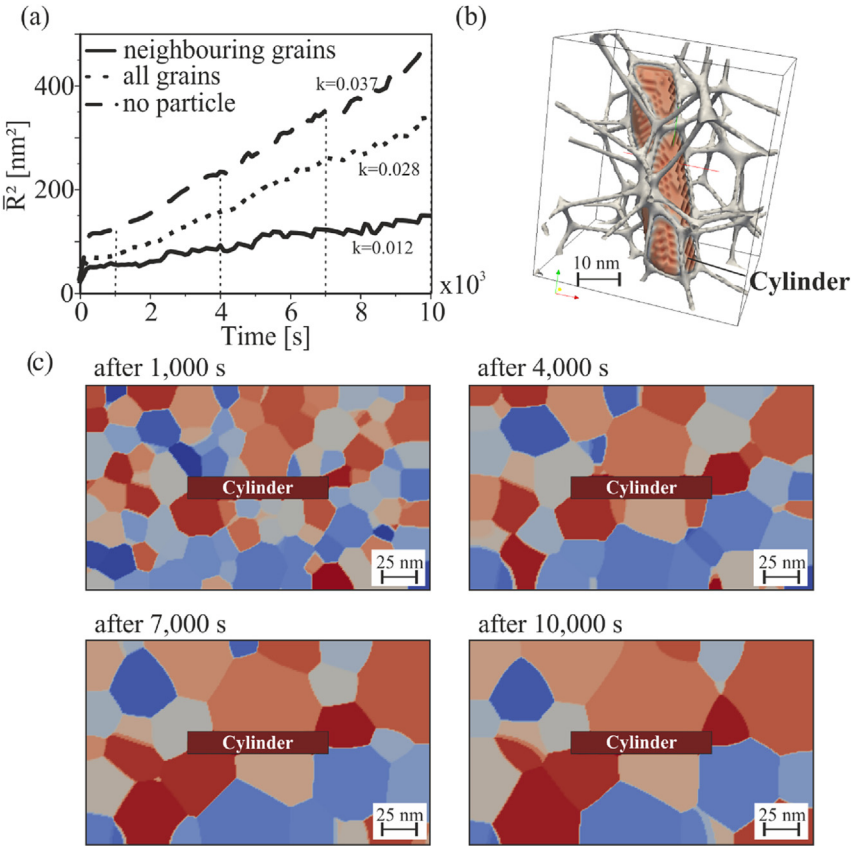

Fig. 6. (a) Average grain size evolution and grain growth coefficient $k(\bar{R}^2 = kt + \bar{R}_0^2)$ of neighbouring grains (around inclusion) and whole simulation box are compared with normal grain growth (no inclusion). (b) Single cylinder within the networks of junctions (grey network shows triple lines and junction points). (c) Slices in cylinder neighbourhood at the indicated times.

total area of the grain boundary tends to be reduced and, on the other hand, the local equilibrium at the junctions (Young's law: the balance between the surface tensions at the junctions [28]) must be fulfilled. The latter results in local curvatures around the particle which acts against area minimization. This leads to a semi-equilibrium state which strongly depends on the orientation angle θ. Note that the overall curvature around the particle cancels out.

The shift of the grain boundary from the centre is measured by the height w (Fig. 3b), and shown as a function of the orientation (Fig. 3c). For $0 < \theta < 25°$, the grain boundary is locally reorientated so that the cylinder is completely in its plane. Above 25°, however, the local bending increases and prevents further local area reduction. Thus, the grain boundary will be just partially in contact with the particle.

3.2. Cylindrical particles at grain boundary and junctions

There are many studies on randomly dispersed or aligned particles and their pinning effect (See for example [29] and references therein). Since particle drag and pinning is a very local effect, we focus on the specific position of particles within a network of grain boundaries. Practically, particles can be sitting in the bulk, on the grain boundary or junctions, depending on the production history. In composite materials produced by premixing and powder metallurgy, strengthening particles remain at the boundaries or junctions [30–32]. Thus, it is crucial to determine whether the different positioning of particles results in different kinetics.

As shown in Fig. 4, a shrinking grain with (a) two and (b) three neighbouring grains and cylindrical particles at specific positions (c: grain boundary, d: triple junction) was simulated. The results show that the pinning effect of cylinders is greater on grain boundaries than on triple junctions in this set-up. The particles on triple junctions have nearly no retarding effect on grain shrinkage. In fact, upon making contact with an inclusion, the triple line decomposes to three individual junctions which can freely move on the surface of the particle (angular freedom). Note that the grain boundary in contact with the particle always has a 90° equilibrium angle with respect to the tangent plane. These particles can remain on the grain boundaries, stabilize the neighbouring triple junction (Fig. 5: final state, bottom), and influence the later evolution of microstructure.

In the other configuration (Fig. 5: top, interaction), when the grain boundaries touch the particles, new triple junctions form which significantly limit the motion of the grain boundary during contact with the particle (Fig. 4b). This, of course, depends on the initial curvature of the grain boundary. When interaction is finished, grain boundaries strive to recover their natural shape and behaviour. Fig. 5 also shows the 3D final state of interaction with the equilibrium angle at triple junctions (120°) and at the surface of particles (90°). An alignment of grain boundary and triple junction with the cylinder axis due to energy minimization can be observed in both cases.

3.3. Single particle in contact with many grains

Long cylindrical particles may also have a non-local effect on more than one grain. In particular, when grains are relatively small in comparison with the cylinder length, there can be a considerable number of junctions and grain boundaries which come into contact with the particles (Fig. 6b). In this case, a combination of grain boundary area reduction and Young's law [28] fulfilment at these junctions can be a determining factor in the grain growth process. To understand this situation, a cylindrical particle sitting between many small grains is simulated. We have compared kinetics of growth for grains close to the particle and for the simulation box as a whole with and without the particle (Fig. 6a).

The results show that although grain growth is still in the parabolic regime, it is strongly retarded close to the particle. In the current configuration, there are few boundaries which might surround the particle. Hence, the most drag force results from the limited motion of junctions on the surface of the particle. In practice it is difficult for a grain boundary to escape the contact with the particle once the equilibrium junction is established. Furthermore, as shown by Chang and coworkers [29], for systems with small grains and long cylindrical particles, there may be a collaborative drag effect if cylinders are close. Our studies (not illustrated here) show clearly that this effect is weak for cylinders, especially when they are used in small volume fractions in the composite materials.

3.4. Polycrystalline composites with many particles

Composites reinforced with 4 vol.% cylindrical particles are simulated. We investigate two specific cases of long (100 nm) and broken (10 nm) cylindrical particles in comparison with spherical particles of equivalent volume to the long cylinders. An initial microstructure close to Hillert's grain size distribution with average grain radius of 9.5 nm is constructed as matrix volume. Thus, the

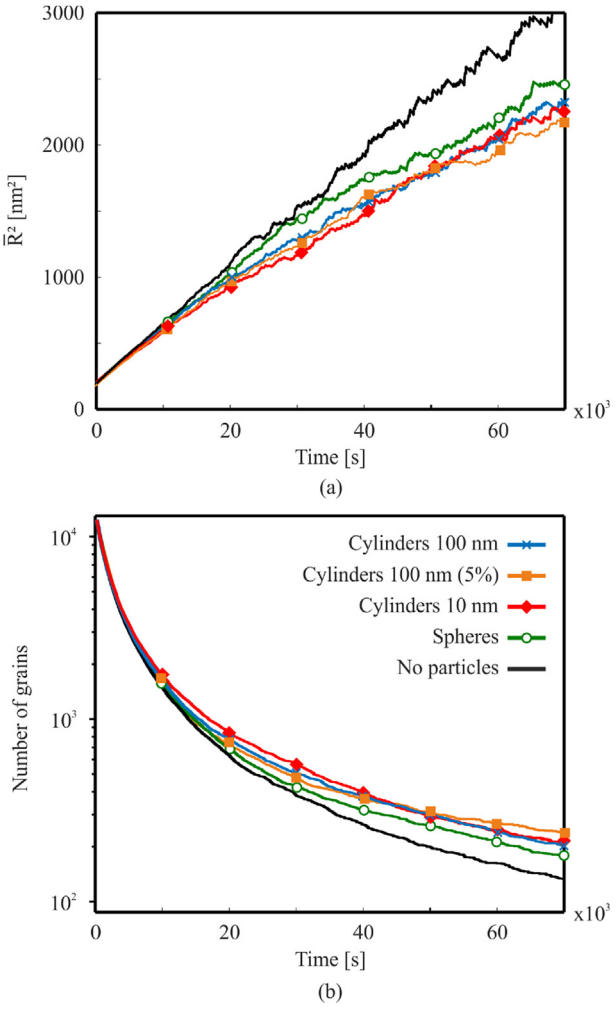

Fig. 7. (a) Kinetics of pinning (spherical particles and cylindrical particles with different length) are compared versus normal grain growth in large 3D systems. (b) Number of grains are shown as a function of time for all simulation boxes. 4 and 5 vol.% particles are simulated.

Table 1
Kinetics equations of growth in the form of $\overline{R}^n = kt + \overline{R}_0^n$. Graphs are shown in Fig. 7a.

Microstructure	Vol.-%	Growth exponent n	Growth coefficient k in nm^n/s
No particles	–	2.031 ± 0.010	0.041 ± 0.002
Spherical particles	4	2.288 ± 0.012	0.107 ± 0.006
Cylindrical particles 100 nm	4	2.491 ± 0.009	0.218 ± 0.008
Cylindrical particles 10 nm	4	2.486 ± 0.014	0.218 ± 0.012
Cylindrical particles 100 nm	5	2.686 ± 0.014	0.452 ± 0.015

shorter cylinders have a volume on the order of that of the grains $\left(\mathrm{Vol}(10\ \mathrm{nm\ cylinder}) = \frac{1}{2}\mathrm{Vol}(\mathrm{grain})\right)$. Fig. 7 shows the evolution of average grain size (a) and the number of grains (b) over time for different simulations. After about 70,000 s the number of grains dramatically decreases and the statistical analysis becomes irrelevant.

The results show that randomly distributed cylindrical particles have a stronger drag and pinning effect than spherical particles and that short and long cylinders have a similar pinning effect. Although longer cylinders are better sites for the formation of immobile junctions as discussed in section (3.3), they are nevertheless few in number. On the other hand, surface-volume ratio favours drag and pinning of smaller cylinders. Increasing the particle fraction to 5 vol.% leads to a more retarded grain growth (Fig. 7a) and a higher remaining grain number (Fig. 7b). No evidence for a collaborative drag effect has been observed for these volume fractions of particles. An orientation alignment of the cylinders in one direction (not shown here) has no special effect on grain growth evolution. The size distribution of the grains (not shown here) was found almost unchanged for all simulations. Table 1 shows information for the growth equation in the form of $\overline{R}^n = kt + \overline{R}_0^n$ with t as time, k as the growth coefficient, and n as the growth exponent. At the presence of particles both exponent and coefficient of growth increases. Smaller simulations boxes with 300^3 grid cells (not shown here) have shown the same tendency of grain growth retardation as observed here.

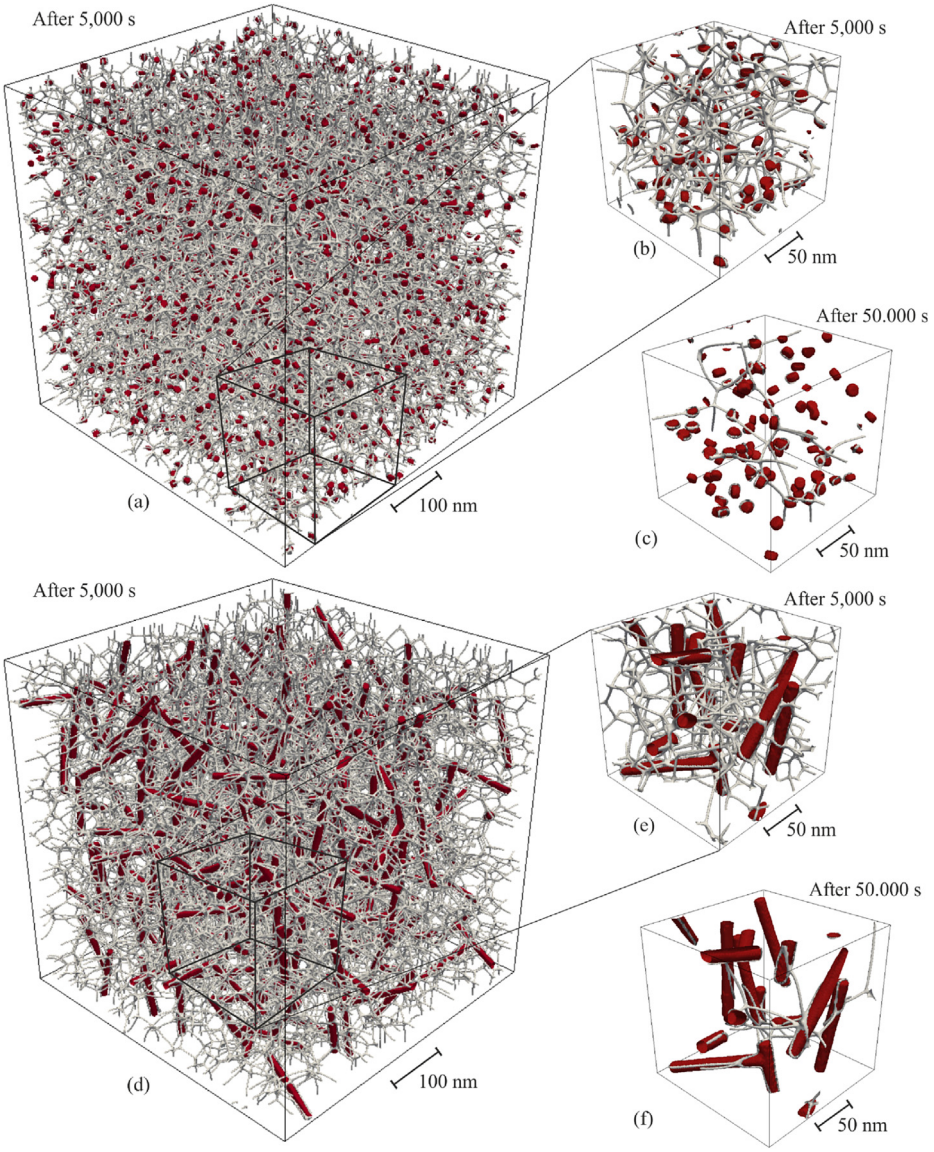

Fig. 8. Simulation boxes after 5000 and 50,000 s for (a,b,c) short and (e,f,g) long cylinders (4 vol.%). Grey network represents triple junctions and vertexes of the grain boundaries. Particles not encased with a grey line lie in the bulk.

Fig. 8 shows the 3D microstructure of the simulation box and an extracted volume after 5000 and 50,000 s. The grey network represents triple junctions or vertexes of higher order. While a small fraction of short cylinders (10 nm) lies on the network (Fig. 8b,c), long cylinders are found to be much more in contact with grain boundaries and junctions (Fig. 8e,f). The persistence of the contacts, however, is not the only determining factor: uniform distribution of short particles, indeed, raises the possibility of frequent interaction which consequently enhances particle drag and pinning.

It is found that during the first stages of grain growth short cylinder's uniform distribution creates the higher pinning effect (Fig. 7a), while at later stages cylinders lying in the bulk region have no influence on pinning. In contrast, long cylinders stay in contact with the grain boundaries and junctions for a long time and can influence the later stages of growth.

4. Conclusion

A systematic study of drag and pinning of cylindrical particles is conducted. We have shown that for a certain combination of grain boundary driving force and particle orientation, a cylindrical particle imposes a higher drag effect than a spherical particle of the same volume. If the misorientation between the grain boundary plane and the cylinder is small, drag force increases and the cylinder can stay in full contact with the grain boundary for a long time. In this case, the grain boundary may only leave the cylindrical particle by large deformations.

A generic drag due to formation of a triple junction on the surface of the particle is characterized. For a cylindrical particle, fulfilling the Young's law at these junctions introduces a new dynamic for the grain boundary and suppresses its kinetics. Within a network of grain boundaries, cylindrical particles have a stronger drag effect on a single grain boundary than on a triple junction. This is due to the angular degree of freedom junctions gain on the surface of the cylindrical particle.

Large-scale simulations with 4 and 5 vol.% particle fraction show that the length of the particles has small influence on the overall drag and pinning. But a stronger pinning effect of cylinders compared to spherical particles is observed. Due to their shape, long cylindrical particles stay much longer in contact with the grain boundary network. This can be of importance in the later stages of growth, where the probability of particle/grain boundary interaction becomes lower.

Acknowledgements

The funding from German Research Foundation (DFG) under grant DA 1655/1-1 within the priority program SPP1713 is highly acknowledged.

References

[1] E.J. Barbero, Introduction to Composite Materials Design, 2, 2010.
[2] A. Kelly, C. Zweben, Comprehensive Composite Materials, 3, Elsevier, 2000.
[3] B.I. Yakobson, P. Avouris, Mechanical properties of carbon nanotubes, Carbon Nanotub. 80 (2001) 287–327.
[4] L. Chunyu, T. Chou, A structural mechanics approach for the analysis of carbon nanotubes, Int. J. Solids Struct. 40 (2003) 2487–2499.
[5] A. Jorio, M.S. Dresselhaus, G. Dresselhaus, Carbon Nanotubes: Advanced Topics in the Synthesis, Structure, Properties and Applications, 2008, pp. 5–6.
[6] J. Hirsch, G. Gottstein, B. Skrotzki, Aluminium Alloys: Their Physical and Mechanical Properties, 2, John Wiley, 2008.
[7] M. Kok, Production and mechanical properties of Al2O3 particle-reinforced 2024 aluminium alloy composites, J. Mater. Process. Technol. 161 (2005) 381–387.
[8] D.J. Lloyd, Particle reinforced aluminium and magnesium matrix composites, Int. Mater. Rev. 39 (1994) 1–23.
[9] N. Moelans, B. Blanpain, P. Wollants, Pinning effect of second-phase particles on grain growth in polycrystalline films studied by 3-D phase field simulations, Acta Mater. 55 (2007) 2173–2182.
[10] Y. Suwa, Y. Saito, H. Onodera, Phase field simulation of grain growth in three dimensional system containing finely dispersed second-phase particles, Scr. Mater. 55 (2006) 407–410.
[11] E. Nes, N. Ryum, O. Hunderi, On the Zener drag, Acta Metall. 33 (1985) 11–22.
[12] N. Ryum, O. Hunderi, E. Nes, On grain boundary drag from second phase particles, Scr. Metall. 17 (1983) 1281–1283.
[13] C.S. Smith, Trans. AIME 175 (1948) 15.
[14] S.P. Ringer, W.B. Li, K.E. Easterling, On the interaction and pinning of grain boundaries by cubic shaped precipitate particles, Acta Metall. 37 (1989) 831–841.
[15] W.B. Li, K.E. Easterling, The influence of particle shape on zener drag, Acta Metallurgica Materialia 38 (1990) 1045–1052.
[16] I. Steinbach, Phase-field model for microstructure evolution at the mesoscopic scale, Annu. Rev. Mater. Res. 43 (2013) 89–107.
[17] I. Steinbach, F. Pezzolla, B. Nestler, M. Seeelberg, R. Prieler, G.J. Schmitz, J.L.L. Rezende, A phase field concept for multiphase systems, Phys. D. Nonlinear Phenom. 94 (1996) 135–147.
[18] I. Steinbach, Phase-field models in material science, Model. Simul. Mater. Sci. Eng. 17 (2009) 31.
[19] W. Guo, I. Steinbach, Multi-phase field study of the equilibrium state of multi-junctions, J. Mater. Res. 4 (2010) 480–485.
[20] W. Guo, R. Spatschek, I. Steinbach, An analytical study of the static state of multi-junctions in a multi-phase field model, Phys. D. Nonlinear Phenom. 240 (2011) 382–388.
[21] R. Darvishi Kamachali, I. Steinbach, 3-D phase-field simulation of grain growth: topological analysis versus mean-field approximations, Acta Mater. 60 (2012) 2719–2728.
[22] R. Darvishi Kamachali, A. Abbondandolo, K.F. Siburg, I. Steinbach, Geometrical grounds of mean field solutions for normal grain growth, Acta Mater. 90 (2015) 252–258.
[23] I. Steinbach, F. Pezzolla, A generalized field method for multiphase transformations using interface fields, Phys. D. 134 (1999) 385–393.
[24] L.E. Murr, Interfacial Phenomena in Metal and Alloys, Addison-Wesley Pub. Co, 1975.
[25] R. Darvishi Kamachali, Grain Boundary Motion in Polycrystalline Materials, Dissertation, Bochum, 2012.
[26] W.W. Mullins, Two-Dimensional Motion of Idealized Grain Boundaries, J. Appl. Phys. 27 (1956) 900.
[27] B. Zhao, G. Gottstein, L.S. Shvindlerman, Triple junction effects in solids, Acta Mater. 59 (2013) 3510–3518.
[28] T. Young, An essay on the cohesion of fluids, Philos. Trans. R. Soc. Lond. 95 (1805) 65.
[29] K. Chang, W. Feng, L.-Q. Chen, Effect of second-phase particle morphology on grain kinetics, Acta Mater. 17 (2009) 5229–5236.
[30] G.-D. Zhan, J.D. Kuntz, J. Wan, A.K. Mukherjee, Single-wall carbon nanotubes as attractive toughening agents in alumina-based nanocomposites, Nat. Mater. 2 (2003) 38–42.
[31] F. Inam, H. Yan, T. Peijs, M.J. Reece, The sintering and grain growth behaviour of ceramic-carbon nanotube nanocomposites, Compos. Sci. Technol. 70 (2010) 947–952.
[32] T. Wei, Z. Fan, G. Luo, F. Wei, A new structure for multi-walled carbon nanotubes reinforced alumina nanocomposites with high strength and toughness, Mater. Lett. 62 (2008) 641–644.